nature geoscience

LETTERS

PUBLISHED ONLINE: 9 MARCH 2015 | DOI: 10.1038/NGEO2381

Amplification of bedrock canyon incision by wind

Jonathan P. Perkins[1]*, Noah J. Finnegan[1] and Shanaka L. de Silva[2]

Bedrock canyons are ubiquitous on Earth and Mars, and river canyon morphology is commonly used to interpret the climatic and tectonic histories of landscapes[1–3]. On both planets, however, many bedrock canyons exist in dry, wind-dominated environments[4–6]. Although wind abrasion can significantly influence the evolution of arid landscapes[4,7], the role of wind in shaping arid bedrock canyon systems is poorly understood and thus typically neglected. Here we exploit a natural experiment on the western slope of the central Andes that allows direct comparison of wind-affected and wind-protected canyons. Through a combined analysis of the morphology of 36 canyons and topographic wind simulations, we show that wind abrasion can amplify bedrock canyon incision rates by an order of magnitude above fluvial rates. Our results imply that wind can extend bedrock canyons—landforms traditionally thought to evolve only from flowing water. Furthermore, our analyses reveal a direct relationship between aerodynamics and landscape evolution on varying scales. Topographic shielding of high winds by mountains modulates the pace of canyon retreat, while individual canyon profiles become aerodynamically streamlined. We conclude that wind abrasion can significantly modify the morphology of bedrock canyons and suggest that wind may have similarly reshaped fluvial landscapes on the martian surface.

On Mars, bedrock canyons are one of the most common tools employed for understanding hydrologic conditions throughout the planet's history[5,6,8–10]. Although most martian canyons are thought to originate from either prolonged surface runoff[6,10], groundwater sapping[8,10], or megafloods[5,11], persistent surface water on Mars vanished at the end of the Hesperian period[12], leaving its surface exposed primarily to atmospheric winds for the past ~3 Gyr. As modern-day wind abrasion rates on Mars are comparable to those on Earth[13], there is potential for substantial modification of martian valley networks by wind (for example, Fig. 1).

In Kasei Valles, for example, flood discharges estimated using canyon geometry are two orders of magnitude larger than any megaflood event measured on Earth[5]. Given that evidence for wind abrasion along the canyon floors of Kasei Valles suggests a deepening of the channel (for example, Fig. 1c) and that the encompassing region has been shown through global climate modelling to exist in a net wind erosional environment for the past 1 Gyr (ref. 15), it is reasonable to suspect wind may have played a role in modifying the channel morphology here. Although wind abrasion may ultimately be less important to shaping Kasei Valles than flood incision, these observations nevertheless provide motivation for exploring the role of aeolian processes in shaping bedrock canyons in arid landscapes.

The 4.09-Myr-old Puripicar ignimbrite[16], located on the western slope of the Andes in northeast Chile (Fig. 2a), provides a natural experiment that isolates the effect of wind abrasion on bedrock canyon morphology. Bounded at its western edge by a ~70 km, north–south-trending escarpment that ranges in height from 15 to 150 m, the Puripicar exhibits a series of ~46 bedrock river gorges that bite into the escarpment along its entire length. Deflection of the zonal westerlies over the Andes[17] results in a regional scale unidirectional wind pattern[17,18] and northwest– southeast-trending wind abrasional features across an array of ignimbrite surfaces spanning 1–5 Myr old from 21° S to 24° S suggest this pattern has been relatively consistent over a very large area since the Pliocene[19].

The southern half of the Puripicar frontal escarpment abuts a prominent ridge of Palaeozoic basement rock that serves to shield the escarpment face from the predominantly northwesterly winds and results in a first-order difference in canyon form (Fig. 2b,c). This natural control allows us to quantify rates of canyon retreat into the frontal escarpment for both the wind-affected and wind-protected populations. Below we discuss the unique conditions of this natural experiment, describe in detail the morphologic evidence for wind-driven canyon retreat and show conceptually

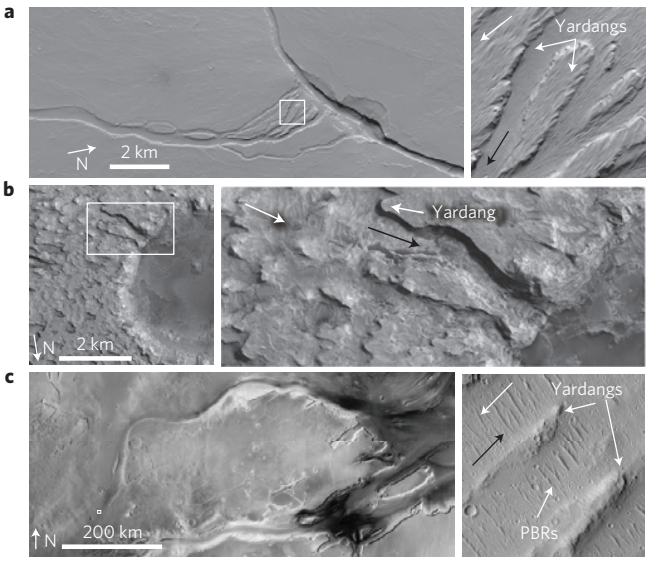

Figure 1 | Satellite images showing evidence for wind abrasion along martian bedrock canyons. White arrows indicate wind direction; black arrows indicate the direction of water flow. **a**, High Resolution Imaging Science Experiment (HiRISE) image PSP_002486_1860 of a channel network near Ascraeus Mons. Islands between the branching channels are evolving into megayardangs. **b**, HiRISE image ESP_013097_1850 shows a canyon entering Crommelin Crater whose headwaters are evolving into a yardang field. **c**, Image of Kasei Valles (ESA ID 292688). Inset image (HiRISE PSP_010462_2035) shows a field of yardangs and periodic bedrock ridges[14] along the broad channel floor oriented opposite the direction of water flow. Images courtesy of: **a**,**b**, NASA/JPL/University of Arizona; **c**, ESA/DLR/FU Berlin.

[1]Department of Earth and Planetary Sciences, University of California Santa Cruz, 1156 High Street, Santa Cruz, California 95064, USA. [2]College of Earth, Ocean, and Atmospheric Sciences, Oregon State University, 104 CEOAS Administration Building, Corvallis, Oregon 97331-5503, USA.
*e-mail: jperkins@es.ucsc.edu

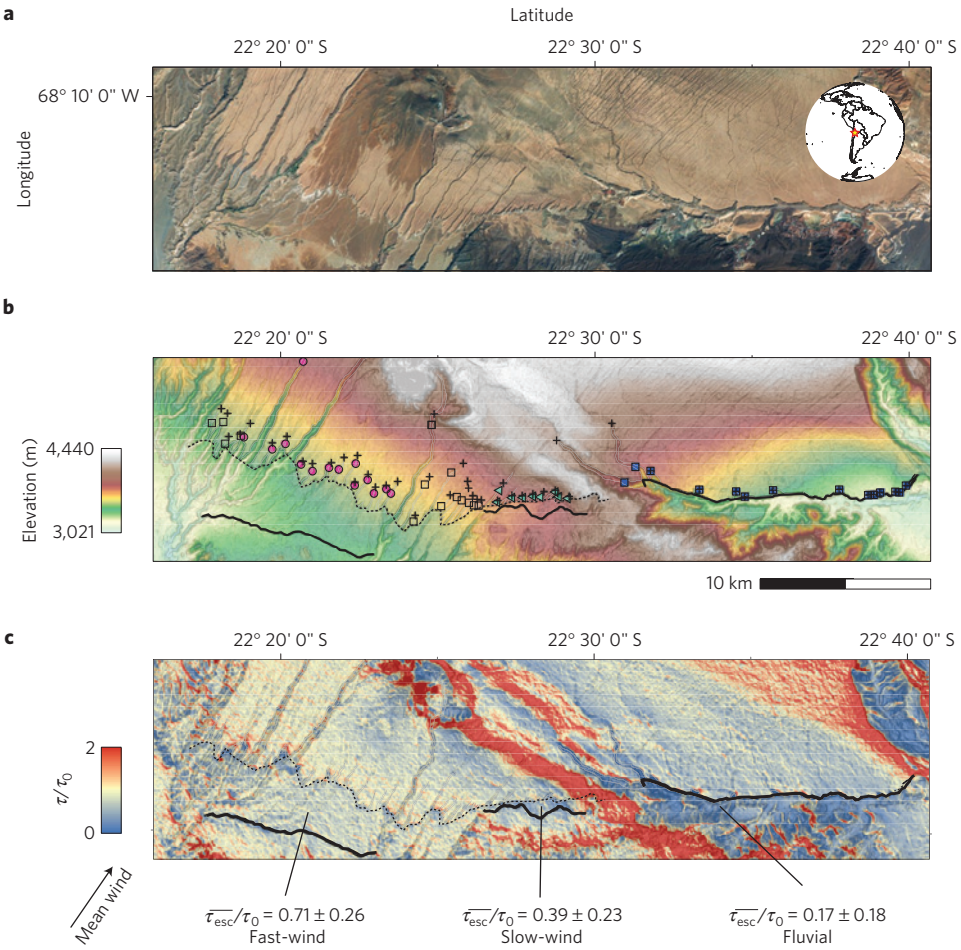

Figure 2 | Overview of the Puripicar frontal escarpment. a, Satellite image showing canyon morphology. **b**, Shaded elevation map derived from ASTER digital elevation model. Magenta circles are canyons in the fast-wind regime; cyan triangles are canyons in the slow-wind regime; blue squares are wind-protected canyons in the fluvial regime. Plus symbols (+) are locations of canyon heads. Open squares are canyons omitted from the analysis. **c**, Results of a topographic wind model[20] run showing normalized surface shear stress with incident winds from the northwest. Labelled values correspond to mean normalized shear stress ($\overline{\tau_{esc}}/\tau_0 \pm 1\sigma$) along each escarpment location. Bold lines correspond to mapped initial escarpment locations. Dotted lines in **b**,**c**, indicate the modern escarpment location. Images courtesy of: **a**, Esri, ArcGIS 10; **b**, ASTER GDEM, a product of METI and NASA.

using a topographic wind model[20] over idealized topography how aerodynamically forced wind abrasion can propagate canyons and streamline them in the process.

The Puripicar is a ~1,400 km^3, crystal-rich dacitic ignimbrite erupted during a phase of intense silicic volcanism within the Central Volcanic Zone of the Andes in the mid-Pliocene epoch[21]. Erupted from the western edge of the Altiplano at ~4,500 m, the pyroclastic flows descended downslope along the western Andean front[21] to an elevation of ~3,500 m. Vapour phase alteration from post-emplacement gas escape resulted in a resistant caprock of several metres in thickness along the Puripicar's upper surface that overlies the much weaker, lower tuff unit[21]. Westerly wind erosion scars the headwaters of the Puripicar along the caprock surface, carving tributaries into a complex suite of wind-parallel streaks and yardangs[19] (Supplementary Fig. 1).

The frontal escarpment of the ignimbrite seems to have initiated from incision into transverse valleys created where the ignimbrite pooled behind local topographic highs (Fig. 2b). The escarpment-perpendicular canyons we observe in the Puripicar are thus probably incising as a transient response to the change in local base level produced by creation of the frontal escarpment shortly after its emplacement. In bedrock river systems, these incisional pulses tend to migrate upstream as kinematic waves referred to as knickpoints[22]. As channels re-adjust to a new equilibrium, knickpoints migrate upstream and canyons propagate farther into the deposit.

We observe, however, a first-order difference in canyon morphology between the northern and southern segments of the Puripicar ignimbrite, suggesting a fundamental change in erosional process that corresponds to the transition from wind-affected to wind-protected canyons (Fig. 2b,c). Canyons along the northern escarpment of the deposit are both more elongate and more v-shaped in plan view than canyons to the south (Fig. 3a,b). The interfluves along the northern section have been characterized as megayardangs that retreat through wind erosion of the lower, weaker tuff and subsequent block collapse of the resistant caprock[23]. Furthermore, geologic and geomorphic evidence suggest portions of the northern escarpment originated more than 3 km to the west at the feet of small transverse ridges (bold lines in Fig. 2 and Supplementary Fig. 2).

Conversely, canyons along the southern 20 km of the Puripicar are stubby in plan view, theatre shaped and nested behind an escarpment that has not retreated far beyond its initial edge (Figs 2b and 3a). The theatre-headed shape and steep headwalls of the southern canyons are consistent with knickpoint retreat from vertical drilling of the weak lower rock and undercutting of the caprock by plunge pool erosion[24]. Although the caprock seems to thicken gradually to the south, this gradual change does not

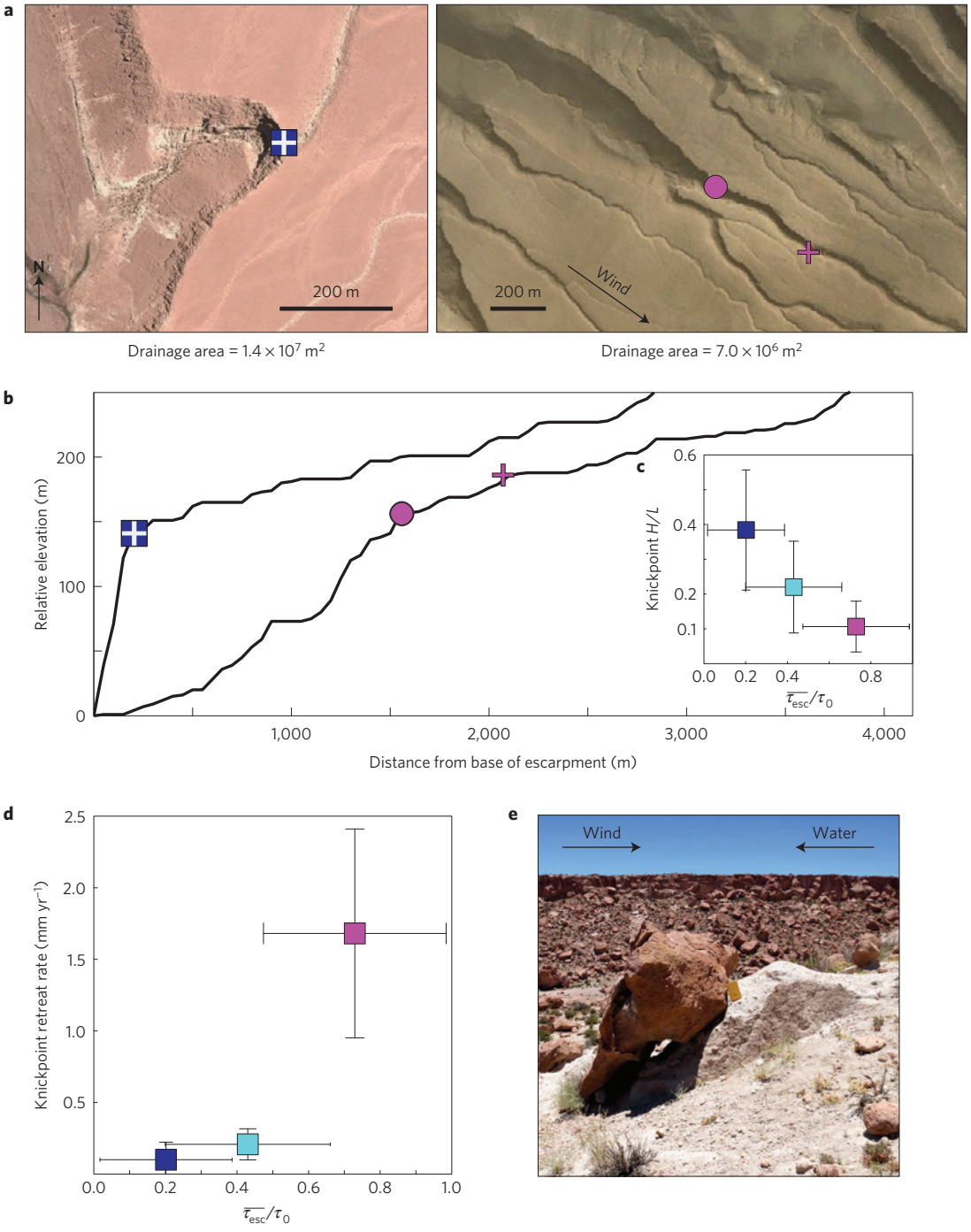

Figure 3 | Comparison between wind-protected and wind-affected channels. Blue, cyan and magenta colours correspond to data from fluvial, slow-wind and fast-wind populations, respectively. Plus symbols are canyon heads; filled shapes are knickpoint crest locations. **a**, Satellite images showing representative shapes of wind-protected and wind-affected canyons of comparable drainage areas. Plus symbols represent canyon heads; shapes correspond to knickpoint crests. **b**, Profiles of channels in **a**. **c**, Mean (±1σ) knickpoint slopes as a function of mean (±1σ) normalized shear stress at the escarpment. **d**, Mean (±1σ) canyon retreat rate as a function of mean (±1σ) normalized escarpment shear stress. **e**, Photo looking across a wind-abraded canyon where a fallen boulder casts an erosional shadow within the weak underlying tuff. Images courtesy of: **a**, Esri, ArcGIS 10; **e**, J. P. Perkins.

correlate spatially with the abrupt change in canyon form and is thus not likely to be a primary control. Here the escarpment is located behind a 500–700 m ridge of Palaeozoic basement rock[21], which acts as a barrier to shield the lower canyon mouths from regional northwesterly winds (Fig. 2c).

Given that lithology and climate do not vary systematically between our two primary populations, we hypothesize that wind abrasion of the exposed knickpoint faces accounts for the morphologic difference in canyons along the escarpment. Supplementary Fig. 3 illustrates how differences in the erosion process between wind and water along the Puripicar yield different predictions of local erosion rate and consequently canyon morphology.

For our topographic analysis we divide canyons into three populations that correspond to our three mapped initial escarpment locations (Fig. 2b). Both canyon head and escarpment retreat distances correlate with topographically forced variations in mean

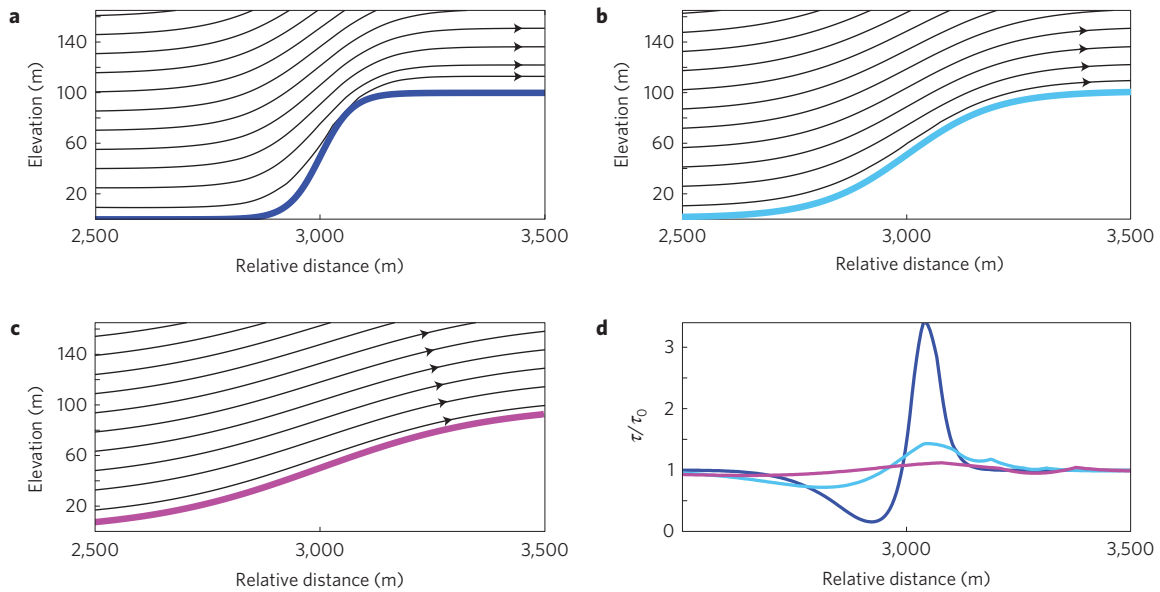

Figure 4 | Results of wind model runs over two-dimensional topographic ramps. a–c, Streamlines for three model runs over sigmoidal ramps with step dimensions equal to the fluvial (**a**), slow-wind (**b**) and fast-wind (**c**) populations. Streamline compression signifies an increase in wind speed. **d**, Associated surface shear stress (τ) normalized to incident shear stress (τ_0) for each topographic profile.

wind shear stress (Fig. 2c). We label these populations fluvial, slow-wind and fast-wind, which correspond to protected, partially protected and unprotected canyons, respectively. We measure along-channel horizontal retreat distances and find that the southern, fluvial canyons are retreating an average of 0.1 ± 0.1 mm yr^{-1}, with knickpoint crests located at the approximate lithologic boundary between the resistant caprock and less indurated basal unit of the tuff (Fig. 3a). The partially protected slow-wind canyon retreat rates increase by a factor of 2 (0.2 ± 0.1 mm yr^{-1}) and the unprotected fast-wind retreat rates increase by a factor of 17 (1.7 ± 0.7 mm yr^{-1}, Fig. 3d). This observed nonlinear dependence of canyon incision on shear stress is consistent with models of wind abrasion by saltating sediment[25,26]. Additionally, wind-affected canyons are ~100 m wider at their mouths for rivers of similar drainage area (Supplementary Fig. 4) and wind-affected canyon heads have uniformly migrated downwind of knickpoint crests (Figs 2b and 3b,d; Supplementary Fig. 5). This suggests that abrasion is occurring along canyon walls as well as above the crests of knickpoints.

We see clear field evidence for aeolian abrasion in wind-affected canyons in the form of erosional shadows where toppled blocks have shielded the underlying tuff from surface deflation (Fig. 3e). Once fallen, the blocks abrade in place, leaving upwind-facing horizontal fingers formed by the preferential erosion of weaker matrix around lithic inclusions (Supplementary Fig. 6). Although the availability of wind-transportable material is scarce, the ignimbrite may provide its own tools for erosion through surface weathering (Supplementary Fig. 7) and abrasion (Supplementary Fig. 6).

An additional topographic signature of this process transition exists in the canyon profile morphology. The mean knickpoint slope measurement in the slow-wind regime is approximately half that of the fluvial regime (0.22 ± 0.13 and 0.39 ± 0.17, respectively) and that in the fast-wind regime is another factor of two less (0.11 ± 0.07, Fig. 3c). The contrast in knickpoint slope and retreat distance between wind-protected and wind-affected canyons suggests that wind abrasion alters canyon morphology by both propagating knickpoints downwind and reducing their slope. We hypothesize that the topographic forcing of wind over a knickpoint leads to enhanced abrasion at its crest and consequently a more aerodynamic canyon geometry. As winds tend to speed up at topographic highs owing to streamline compression[27], and wind abrasion rate is extremely sensitive to changes in boundary shear stress[25,26], topography should exert an influence on local wind abrasion rates.

We show this effect through wind model simulations over idealized topography with representative step dimensions from our fluvial, slow-wind and fast-wind populations (Fig. 4; Supplementary Fig. 8; see Methods for model information). Steep-sloping fluvial knickpoints produce a threefold increase in normalized wind surface shear stress at the knickpoint crest (Fig. 4d). Erosion will thus focus along the crest due to the nonlinear dependence of abrasion rate on shear stress[25]. This speed-up effect diminishes significantly for representative canyons in the slow-wind regime and all but disappears for slopes in the fast-wind regime (Fig. 4). A constant shear stress distribution across the fast-wind profile suggests these canyons represent equilibrium shapes (that can still propagate downwind), whereas the wind-protected fluvial profiles are highly unstable within a wind abrasion regime.

Taken together, our results show that topography influences wind-driven landscape evolution on varying scales: topographic shielding of high wind potential by mountains modulates the pace of canyon retreat along the Puripicar, whereas enhanced wind shear over knickpoints governs local abrasion rate within individual canyons. Although our results suggest wind-affected canyons seem to have a distinct topographic signature, fluvial knickpoint morphology can also vary greatly depending on the erosion process[28] and therefore shallow knickpoint geometries are not a unique indicator of the wind abrasion process. However, large regions of both Mars and Earth contain evidence of bedrock abrasion by wind[4,7], and within these landscapes wind may contribute significantly to landscape evolution through the abrasion of arid canyon systems. Furthermore, windblown sediment transport through canyons may not coincide with the fluvial transport direction and may potentially complicate sediment routing and budgets.

On Mars, many valley networks are commonly located near zones of high wind abrasion potential[15]. Thus present channel forms may not accurately reflect the fluvial processes that initially carved them. As wind has the potential to significantly alter channel

morphology by both widening and deepening, palaeohydrologic reconstructions from ancient martian channels may require additional constraints to account for the potential effect of persistent wind abrasion. We note that yardang canyons in the Puripicar ignimbrite evolved while rivers have actively contributed to canyon incision. This overprinting of process makes wind-abraded canyons difficult to identify and highlights the possibility that even when water was present on the martian surface, wind may still have contributed to canyon formation. Determining the intermittency of both surface water and wind sediment transport events should aid in determining the relative contribution of these processes in arid, windy canyon systems.

Methods

Mapping the Puripicar ignimbrite's initial windward escarpment position. We map the initial position of the escarpment using the following lines of evidence. First, across the entire deposit, the ignimbrite seems to have terminated by pooling behind local topographic highs (Fig. 2b). A natural consequence of this pooling is the creation of valleys parallel to the margin of the deposit along the base of the topographic ridge. Surface water gets channelled along this margin, providing a mechanism to generate relief and form an escarpment. Second, the ignimbrite surface behind the wind-affected escarpment projects directly to the escarpment-parallel valley axis approximately 3 km upwind. Supplementary Fig. 2 shows the downslope projection of a one-dimensional best-fit quadratic polynomial through the upper ignimbrite surface ($R^2 = 0.99$). We map two locations where the Puripicar seems to have initially pooled at the base of a local ridge (Fig. 2b).

Analysis of canyon incision using topographic and imagery data. We identify 46 bedrock canyons along the Purpicar modern frontal escarpment using both Worldview satellite imagery and Advanced Spaceborne Thermal Emission and Reflection Radiometer (ASTER) elevation data, and restrict our analysis to 36 canyons that correlate to our mapped initial escarpment locations. To quantify canyon incision rates for each channel we measure the horizontal along-channel distance that each knickpoint has migrated behind its mapped initial escarpment ($\Delta x = x_{\text{final}} - x_{\text{initial}}$) and divide by the age of the deposit[16] (T), assuming that creation of the escarpment occurred shortly after emplacement of the ignimbrite. We map channel pathways using a flow-routing algorithm within ArcGIS and identify knickpoint crests as the large downstream break in slope along each channel's longitudinal profile (for example, Fig. 3b). We calculate upstream drainage area at each knickpoint crest using a flow-accumulation tool within ArcGIS. Supplementary Fig. 4 shows the distribution of drainage areas for both the windward and wind-shielded canyons. The range of drainage areas between wind-affected and wind-protected populations overlaps nearly completely, indicating that drainage area differences are probably not responsible for the discrepancy in knickpoint retreat rates between the two populations. We divide our canyons into three populations: fluvial, slow-wind and fast-wind, which correspond to broad zones along the Puripicar's frontal escarpment whose mean normalized shear stress values in front of the escarpment ($\overline{\tau_{\text{esc}}}/\tau_0$) differ significantly as a result of shielding by large topographic obstacles. We calculate knickpoint slopes by measuring the approximate vertical and horizontal step dimensions along each channel. We first mark the upper and lower bounds of the step by hand, which we identify as marked deviations in channel slope from the upstream and downstream channel segments (for example, Fig. 3b). We then measure the absolute vertical (H) and horizontal (L) distances between the upper and lower bounds of the step, and take the knickpoint slope as the ratio H/L.

Using Worldview-1 satellite imagery within ArcGIS, we identify canyon heads as locations where channel walls begin to substantially widen towards the escarpment (for example, Fig. 3a,b). Wind-protected canyon heads are co-located with topographic knickpoint crests (Fig. 3a). Wind-affected canyon heads are located downwind of topographic knickpoint crests and correspond to the upper-most fracture plane in the caprock where blocks are being delivered to the channel (Supplementary Fig. 5). We estimate variations in canyon width between our windward and wind-protected canyons by measuring across-canyon horizontal distance along the modern escarpment.

Topographic wind modelling. We use a mass-conserving topographic wind model (WindNinja[20]) together with a 30 m ASTER digital elevation model to constrain the influence of large topographic structures on the regional wind field across the Puripicar ignimbrite's frontal escarpment. As we are interested primarily in the relative change of surface shear stress induced by topography, we normalize all shear stress measurements to the upstream flow condition in our model, and use generic values of incident shear velocity and surface roughness (1.0 m s^{-1} and 0.01 m, respectively). We assign an incident wind direction of 305°, parallel to wind abrasion features along the Puripicar surface and consistent with measurements of palaeowind direction across the central Andes since the Pliocene[19].

We model wind speed variations over knickpoint topography by generating two-dimensional sigmoidal ramps of the form $1/(1+ce^{-x})$, where c is a constant that governs the slope magnitude. We use step dimensions equal to our fluvial, slow-wind and fast-wind populations (for example, Supplementary Fig. 8).

We estimate local surface shear stress by measuring the vertical gradient in velocity, for example[29]:

$$\frac{\tau}{\tau_0} \approx \lim_{z \to 0} (1 + \Delta s)^2$$

where

$$\Delta s = \frac{u(x,z)}{u(x_0, z - hf(x))} - 1$$

is the fractional speed-up ratio[27] directly above the bed and $hf(x)$ is the elevation of the bed topography. We measure velocity speed-up (Δs) at $z = 10$ cm and normalize the measurements to our upstream flow condition along a flat surface (τ_0).

ASTER topographic data is publicly available and can be found at gdem.ersdac.jspacesystems.or.jp. Data from our topographic analysis is available as a spreadsheet within our Supplementary Table 1. WindNinja is freely available at http://www.firelab.org/project/windninja. Esri images are from ArcGIS version 10 (http://services.arcgisonline.com/ArcGIS/rest/services/World_Imagery/MapServer).

Received 22 June 2014; accepted 2 February 2015; published online 9 March 2015

References

1. Ferrier, K., Huppert, K. & Perron, J. Climatic control of bedrock river incision. *Nature* **496,** 206–209 (2013).
2. Howard, A. D., Dietrich, W. E. & Seidl, M. A. Modeling fluvial erosion on regional to continental scales. *J. Geophys. Res.* **99,** 13971–13986 (1994).
3. Schoenbohm, L. M., Whipple, K. X., Burchfiel, B. C. & Chen, L. Geomorphic constraints on surface uplift, exhumation, and plateau growth in the Red River region, Yunnan Province, China. *Geol. Soc. Am. Bull.* **116,** 895–909 (2004).
4. Goudie, A. S. Mega-Yardangs: A global analysis. *Geography Compass* **1,** 65–81 (2007).
5. Baker, V. Water and the martian landscape. *Nature* **412,** 228–236 (2001).
6. Howard, A. D., Moore, J. M. & Irwin, R. P. An intense terminal epoch of widespread fluvial activity on early Mars: 1. Valley network incision and associated deposits. *J. Geophys. Res.* **110,** E12S14 (2005).
7. McCauley, J. F. Mariner 9 evidence for wind erosion in the equatorial and mid-latitude regions of Mars. *J. Geophys. Res.* **78,** 4123–4137 (1973).
8. Pieri, D. Martian valleys: Morphology, distribution, age, and origin. *Science* **210,** 895–897 (1980).
9. Carr, M. H. & Clow, G. D. Martian channels and valleys: Their characteristics, distribution, and age. *Icarus* **48,** 91–117 (1981).
10. Aharonson, O., Zuber, M., Rothman, D., Schorghofer, N. & Whipple, K. Drainage basins and channel incision on Mars. *Proc. Natl Acad. Sci. USA* **99,** 1780–1783 (2002).
11. Lamb, M., Dietrich, W., Aciego, S., Depaolo, D. & Manga, M. Formation of Box Canyon, Idaho, by megaflood: Implications for seepage erosion on Earth and Mars. *Science* **320,** 1067–1070 (2008).
12. Carr, M. H. & Head, J. W. Geologic history of Mars. *Earth Planet. Sci. Lett.* **294,** 185–203 (2010).
13. Bridges, N. *et al.* Earth-like sand fluxes on Mars. *Nature* **485,** 339–342 (2012).
14. Montgomery, D. R., Bandfield, J. L. & Becker, S. K. Periodic bedrock ridges on Mars. *J. Geophys. Res.* **117,** E03005 (2012).
15. Armstrong, J. & Leovy, C. Long term wind erosion on Mars. *Icarus* **176,** 57–74 (2005).
16. Salisbury, M. J. *et al.* ^{40}Ar/^{39}Ar chronostratigraphy of Altiplano–Puna volcanic complex ignimbrites reveals the development of a major magmatic province. *Geol. Soc. Am. Bull.* **123,** B30280 (2010).
17. Vuille, M. Atmospheric circulation over the Bolivian Altiplano during dry and wet periods and extreme phases of the Southern Oscillation. *Int. J. Climatol.* **19,** 1579–1600 (1999).
18. Kreuels, R., Fraedrich, K. & Ruprecht, E. An aerological climatology of South America. *Meteorol. Rundsch.* **28,** 17–24 (1975).
19. Bailey, J. E., Self, S., Wooller, L. K. & Mouginis-Mark, P. J. Discrimination of fluvial and eolian features on large ignimbrite sheets around La Pacana Caldera, Chile, using Landsat and SRTM-derived DEM. *Remote Sens. Environ.* **108,** 24–41 (2007).

20. Forthofer, J. M., Butler, B. W. & Wagenbrenner, N. S. A comparison of three approaches for simulating fine-scale surface winds in support of wildland fire management. Part I. Model formulation and comparison against measurements. *Int. J. Wildland Fire* **23,** 969–981 (2014).
21. De Silva, S. L. Geochronology and stratigraphy of the ignimbrites from the 21°30′S to 23°30′S portion of the central Andes of northern Chile. *J. Volcanol. Geotherm. Res.* **37,** 93–131 (1989).
22. Seidl, M. & Dietrich, W. The problem of channel erosion into bedrock. *Catena Supp.* **23,** 101–124 (1993).
23. De Silva, S. L., Bailey, J. E., Mandt, K. E. & Viramonte, J. M. Yardangs in terrestrial ignimbrites: Synergistic remote and field observations on Earth with applications to Mars. *Planet Space Sci.* **58,** 459–471 (2010).
24. Lamb, M. P., Howard, A. D., Dietrich, W. E. & Perron, J. T. Formation of amphitheater-headed valleys by waterfall erosion after large-scale slumping on Hawai'i. *Geol. Soc. Am. Bull.* **119,** 805–822 (2007).
25. Anderson, R. S. Erosion profiles due to particles entrained by wind: Application of an eolian sediment-transport model. *Geol. Soc. Am. Bull.* **97,** 1270–1278 (1986).
26. Greeley, R. *et al.* Rate of wind abrasion on Mars. *J. Geophys. Res.* **87,** 10009–10024 (1982).
27. Jackson, P. S. & Hunt, J. C. R. Turbulent wind flow over a low hill. *Q. J. R. Meteorol. Soc.* **101,** 929–955 (1975).
28. Weissel, J. K. & Siedl, M. A. in *Rivers Over Rock: Fluvial Processes in Bedrock Channels* Vol. 107 (eds Tinkler, K. J. & Wohl, E. E.) 189–206 (American Geophysical Union, 1998).
29. Deaves, D. M. Wind over hills: A numerical approach. *J. Ind. Aerodyn.* **1,** 371–391 (1975).

Acknowledgements

We thank K. Johnson and D. M. Rubin for field assistance and discussions that helped improve this manuscript. We thank H. T. Rivadera for logistical support in Chile and N. Wagenbrenner for help with wind modelling. This work was financially supported by National Science Foundation grants EAR 0908850 (N.J.F.), EAR 0908324 (S.L.d.S.) and NASA NNX10AP79G (S.L.d.S.).

Author contributions

J.P.P. and N.J.F. designed the study with the help of S.L.d.S., who provided observations and field guidance that motivated ideas in this manuscript. J.P.P. analysed topography and model data with input from N.J.F. All authors collected field data and edited the manuscript, which was written by J.P.P.

Additional information

Supplementary information is available in the online version of the paper. Reprints and permissions information is available online at www.nature.com/reprints. Correspondence and requests for materials should be addressed to J.P.P.

Competing financial interests

The authors declare no competing financial interests.